Available online at www.sciencedirect.com
SCIENCE DIRECT
Engineering Geology 83 (2006) 144–160
ENGINEERING GEOLOGY
www.elsevier.com/locate/enggeo

Large rock avalanches triggered by the M 7.9 Denali Fault, Alaska, earthquake of 3 November 2002

Randall W. Jibson [a,*], Edwin L. Harp [a], William Schulz [a], David K. Keefer [b]

[a] U.S. Geological Survey, Box 25046, MS 966, Denver Federal Center, Denver, CO 80225, USA
[b] U.S. Geological Survey, 345 Middlefield Rd., MS 977, Menlo Park, CA 94025, USA

Accepted 24 June 2005
Available online 15 December 2005

Abstract

The moment magnitude (**M**) 7.9 Denali Fault, Alaska, earthquake of 3 November 2002 triggered thousands of landslides, primarily rock falls and rock slides, that ranged in volume from rock falls of a few cubic meters to rock avalanches having volumes as great as 20×10^6 m^3. The pattern of landsliding was unusual: the number and concentration of triggered slides was much less than expected for an earthquake of this magnitude, and the landslides were concentrated in a narrow zone about 30-km wide that straddled the fault-rupture zone over its entire 300-km length. Despite the overall sparse landslide concentration, the earthquake triggered several large rock avalanches that clustered along the western third of the rupture zone where acceleration levels and ground-shaking frequencies are thought to have been the highest. Inferences about near-field strong-shaking characteristics drawn from interpretation of the landslide distribution are strikingly consistent with results of recent inversion modeling that indicate that high-frequency energy generation was greatest in the western part of the fault-rupture zone and decreased markedly to the east.

Keywords: Earthquake-triggered landslides; Rock avalanche; Earthquake shaking; Alaska

1. Introduction

South-central Alaska and the Alaska Range were severely shaken on the morning of 3 November 2002 by a moment magnitude (**M**) 7.9 earthquake (Fig. 1). The quake triggered about 340 km of surface rupture along the Susitna Glacier, Denali, and Totschunda Faults (Haeussler et al., 2004). Seismic shaking triggered numerous landslides and liquefaction failures within the central part of the Alaska Range and the surrounding region (Eberhart-Phillips et al., 2003; Harp et al., 2003; Jibson et al., 2004; Kayen et al., 2004). Landslides triggered by the earthquake were mainly rock falls and rock slides (landslide terminology after Varnes, 1978) containing mixtures of fractured rock, soil, ice, and snow. The most spectacular landslides triggered by the shaking were large rock avalanches having volumes of several million cubic meters that were deposited on the Black Rapids, McGinnis, and West Fork Glaciers.

Quantifying the near-field strong-motion characteristics for this earthquake has been very difficult because only one strong-motion seismometer was present in the near field. Thus, analysis of the pattern of triggered landslides and liquefaction effects may provide some of the best evidence of the characteristics of the strong shaking.

Previously published papers discussing these landslides (Eberhart-Phillips et al., 2003; Harp et al., 2003;

* Corresponding author. Mailing address (FedEx, etc.): U.S. Geological Survey, 1711 Illinois St., Golden, CO 80401, USA. Tel.: +1 303 273 8577; fax: +1 303 273 8600.
E-mail address: jibson@usgs.gov (R.W. Jibson).

0013-7952/$ - see front matter © 2005 Elsevier B.V. All rights reserved.
doi:10.1016/j.enggeo.2005.06.029

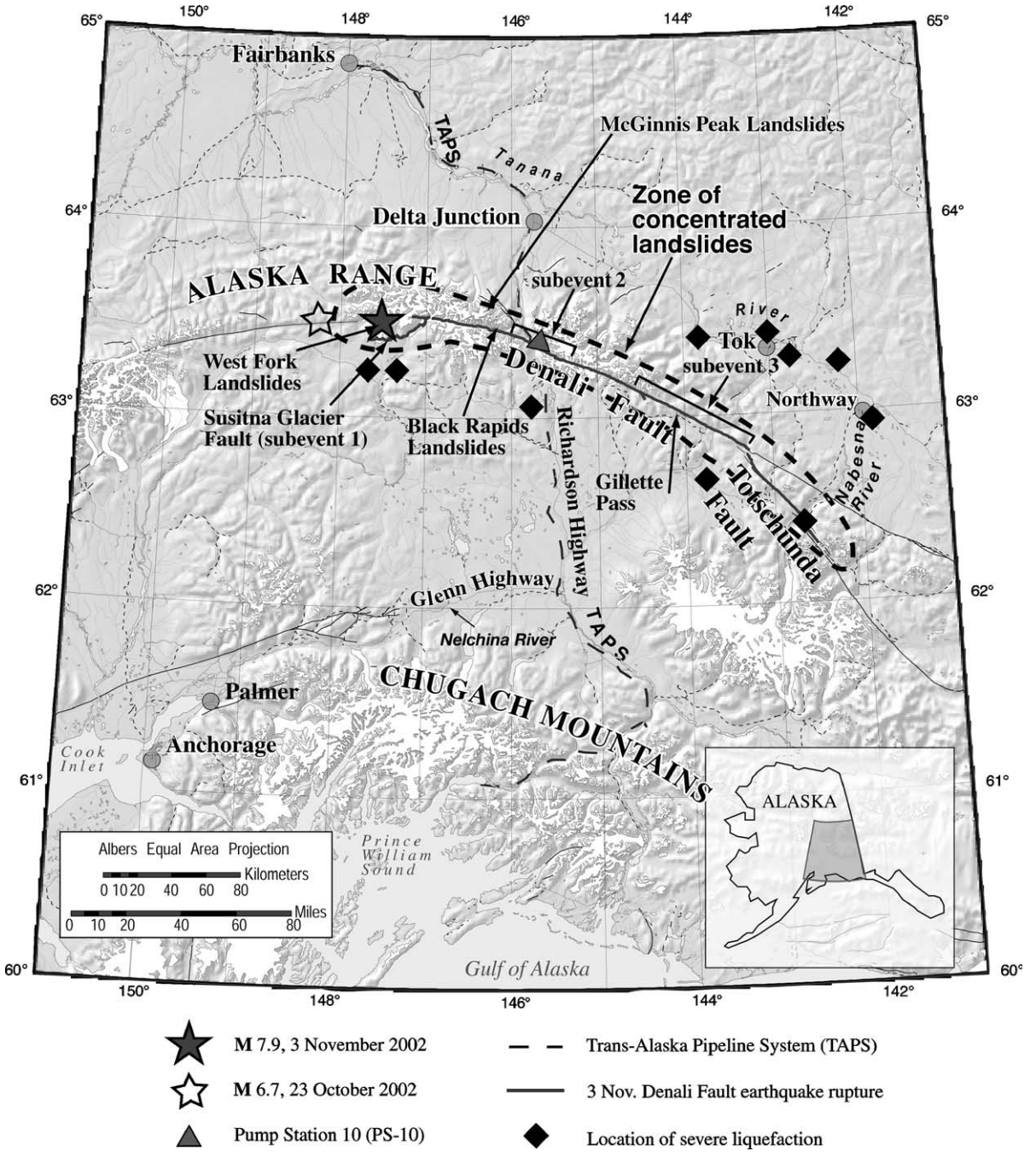

Fig. 1. Map showing area of Denali Fault earthquake. Area enclosed by heavy dashed line shows zone of concentrated landslides triggered by the 2002 earthquake. Earthquake subevent locations from Frankel (2004); liquefaction locations from Kayen et al. (2004).

Jibson et al., 2004) contain estimates of volumes, distances, etc. that were based on initial reconnaissance observations. We have since updated many of these estimates based on additional field work and analysis; thus, values in this paper supersede those published earlier.

In this paper, we briefly describe the faulting and seismological properties associated with the earthquake, characterize the regional distribution of landslides, describe the largest landslides triggered, and interpret the triggered landslides in terms of what they tell us about the distribution and char-

acteristics of strong motion associated with this earthquake.

2. The 3 November 2002 earthquake

The 3 November 2002 earthquake, one of the largest earthquakes in U.S. history, resulted primarily from right-lateral movement on the Denali–Totschunda fault system and associated thrusting along the Susitna Glacier Fault (Fig. 1). The Denali Fault is one of the longest strike-slip fault systems in the world; it consists of numerous strands along its 2000-km length and is comparable in size to the San Andreas Fault that produced the **M** 7.9 San Francisco earthquake of 1906 (Miller et al., 2002). The Totschunda Fault, a major splay of the Denali fault system, extends ~200 km from the U.S.–Canada border northwest to its junction with the Denali Fault at Mentasta Pass (Plafker et al., 1994, 1977). The Denali and Totschunda Faults both show evidence of recent movement. The Susitna Glacier Fault was previously unrecognized.

The **M** 7.9 mainshock was preceded by a **M** 6.7 foreshock on 23 October 2002 on the Denali Fault (Hansen and Ratchkovski, 2004). The epicenter of the mainshock was about 25 km east of the foreshock. The mainshock consisted of multiple subevents—distinct rupture events within the overall earthquake rupture sequence (Kikuchi and Yamanaka, 2002; Frankel, 2004). The first subevent was a **M** 7.2 thrust event on the Susitna Glacier Fault. This event then triggered a second subevent, a **M** 7.3 right-lateral rupture on the Denali Fault centered near the Richardson Highway and Trans-Alaska Pipeline. During a third subevent (**M** 7.6), right-lateral rupture propagated eastward along the Denali Fault for 225 km (Frankel et al., 2002) and continued for about 50 km southeastward on the Totschunda Fault. Right-lateral slip averaged about 3.5 m and ranged from 0.5 to almost 9 m. A maximum of about 3 m of vertical movement occurred as both thrust and normal slip. Pre-existing, degraded fault scarps (Plafker et al., 1977) re-ruptured at many places during the 3 November event.

Only one strong-motion seismometer was operating in the near-field area of the earthquake. Located at Pump Station 10 along the Trans-Alaska Pipeline (Fig. 1), this instrument recorded a peak ground acceleration (PGA) of 0.36 *g* (Ellsworth et al., 2004; Martirosyan et al., 2004). Other seismometers recorded the earthquake at several locations including Anchorage, Fairbanks, and Valdez. These more distant recordings allowed identification of subevents but were too far away to provide much useful information regarding near-field ground accelerations.

3. Distribution and types of triggered landslides

The earthquake triggered thousands of landslides from the steep slopes of the Alaska Range. The distribution of landslides was mapped by aerial reconnaissance. The landslides ranged in size from rock falls of a few cubic meters to rock avalanches of several million cubic meters that were triggered from steep rock slopes bordering large valley glaciers. The large majority of landslides were shallow rock falls and rock slides from steep slopes. Most slopes in the epicentral area have exposures of weathered bedrock or thin colluvium; landslides generally involved failure of the uppermost few decimeters to meters of this material, which cascaded down the steep slopes (Fig. 2). At the time of the earthquake, most slopes were covered by a thin blanket

Fig. 2. Scattered rock falls (examples shown by arrows) on slopes near the Denali Fault. The concentration and size of such rock falls were relatively low for a **M** 7.9 earthquake.

of snow, and so recent landslides were easily identifiable against the white background of the fresh snow.

One unusual aspect of the landslides triggered by this earthquake was their narrow concentration along the fault rupture. Normally, an earthquake of this magnitude would be expected to trigger landslides over a very broad region extending perhaps 350 km from the fault and covering an area of 28,000 to perhaps 90,000 km^2 (Keefer, 1984, 2002). In this earthquake, the large majority of landslides clustered in a narrow band, about 30-km wide, that straddles the fault for more than 300 km (Fig. 1). The largest landslides (described in the following section) clustered at the western part of the fault zone between subevents 1 and 2 (Fig. 1), and landslide concentration decreased eastward along the fault zone. We saw only a few scattered landslides at greater distances from the fault despite the fact that steep, highly susceptible slopes are abundant well beyond the observed 15-km limit on each side of the fault. The most distant triggered landslide we observed was a single rock fall in the Chugach Mountains near Palmer, Alaska, about 250 km southwest of the fault. Also, we saw several failures in sensitive clay along terraces of the Nelchina River about 150 km from the fault. Other than these few landslides, however, we saw no others at distances greater than about 15 km from the fault zone.

Another unusual aspect of the landslides triggered by this earthquake was their relative scarcity. Keefer (2002) examined data from 11 earthquakes for which detailed landslide inventories were compiled and plotted magnitude versus number of landslides triggered. His data suggest that a **M** 7.9 earthquake might be expected to trigger about 80,000 landslides. Although we were unable to compile a detailed inventory, the number of triggered landslides from the Denali Fault earthquake appeared to be at least an order of magnitude less than this. Likewise, landslide concentrations on the steep slopes near the fault were not as great as what we have seen in other recent earthquakes of smaller magnitude, as detailed subsequently in the Discussion.

4. Large rock avalanches

By far the most impressive landslides triggered were several large rock avalanches that spilled onto glaciers in the Alaska Range. Similar avalanches of rock and ice were triggered in the Chugach Range by the 1964 **M** 9.2 Alaska earthquake (Tuthill and Laird, 1966; Post, 1967). All of the largest 2002 rock avalanches were located near the fault ruptures between the first and second subevents. Two of the large rock avalanches occurred near subevent 1 on the hanging wall of the Susitna Glacier thrust fault. The other five large rock avalanches occurred between subevents 1 and 2 on the flanks of McGinnis Peak and on slopes along the south margin of the Black Rapids Glacier. Table 1 shows the geometric characteristics of the largest rock avalanches, and Fig. 3 shows profiles of the pre-existing topography along landslide source areas and paths.

4.1. McGinnis Peak rock avalanches

The earthquake triggered two huge avalanches of rock and ice from different flanks of McGinnis Peak (Figs. 1 and 4, Table 1). The larger northern failure involved more than 20×10^6 m^3 of metamorphic rock and glacial ice (about 10% by volume) that collapsed from the northeast ridge of McGinnis Peak, struck the glacier below the rock face, and then flowed about 11 km down the glacial surface, which has an average surface slope of about 5° (Fig. 5).

The source of the landslide is a near-vertical rock face nearly 1000 m high (Fig. 6). The source rock is predominantly a dense, greenish-gray, fine-grained metamorphic rock. The source scar is defined by a

Table 1
Average geometric characteristics of rock avalanches triggered by the Denali Fault earthquake

Landslide	Vertical drop (km)	Length (km)	Width (km)	Length/height ratio	Source area (km^2)	Deposit area (km^2)	Depth (m)	Volume ($\times 10^6$ m^3)
McGinnis Peak Glacier								
North	1.65	11.0	1.5	6.67	0.40	10.21	2	20.4
South	1.80	11.5	0.7	6.39	0.48	5.71	2	11.4
Black Rapids Glacier								
East	0.98	4.6	1.6	4.69	0.66	4.64	3	13.9
Middle	0.80	4.5	1.2	5.63	0.79	4.55	3	13.6
West	0.73	3.2	1.0	4.38	0.52	3.24	3	9.7
West Fork Glacier								
North	0.76	3.3	0.7	4.34	0.42	1.37	3	4.1
South	0.90	4.1	0.8	4.56	0.55	1.47	3	4.4

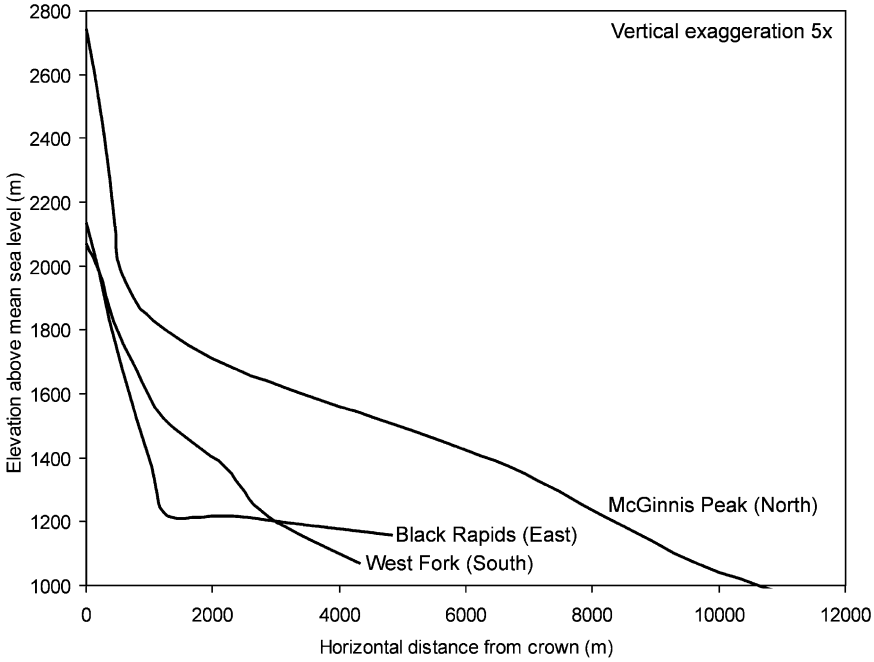

Fig. 3. Topographic profiles of the pre-landslide ground surface for three of the large rock avalanches triggered by the 2002 Denali Fault, Alaska earthquake. Vertical exaggeration is a factor of 5.

planar, nearly vertical, slope-parallel joint surface. The surface is stepped, indicating a series of slope-parallel joints spaced a few meters apart. Above the rock scar is a vertical exposure of 15–20 m of glacial ice, which also failed and became part of the avalanche. At the base of the source slope is a deeply scoured bowl-shaped pit some hundreds of meters across where the rock and ice from above struck the glacial surface in free-fall.

The valley walls near the source are nearly vertical and parallel, and they channeled the failed rock and ice directly down the valley on the glacial surface (Fig. 6). Snow 50–70 m high on valley walls was covered with dust, indicating that the landslide generated a thick dust plume in front of it (see Fig. 6).

About 4 km from the source, landslide debris topped a 150 m high ridge on the left margin of the glacier. This overtopped feature allows us to estimate the minimum velocity of the rock avalanche by applying an equation proposed by Chow (1959) that is commonly used for such estimates (e.g., Evans et al., 2001; Vallance and Scott, 1997; Voight and Sousa, 1994):

$$v = (2gh)^{0.5}, \tag{1}$$

where v is velocity in meters per second, h is runup height in meters, and g is gravitational acceleration (9.81 m/s^2). This equation was developed assuming that gravitational force is the only force resisting flow, hence the velocity obtained using Eq. (1) is the minimum required for a flow to climb to a certain height until stopping due solely to gravitational resistance. Velocity estimates would certainly be greater if other forces resisting flow, such as interparticle frictional and collisional forces and those between the flow and the substrate, were considered. For a 150 m high ridge, Eq. (1) yields a minimum velocity of 54 m/s or about 200 km/h. Because the debris completely overtopped the ridge without deflection and continued down the valley indicates that the velocity was significantly greater than this minimum required to reach the top of the ridge.

At 5 km from the source, the valley turns 70° to the east (Fig. 7). The avalanche debris followed this turn and flowed about 60 m up the valley walls on the outside of the turn, indicating both high velocity and a very fluid type of movement. This presents another opportunity to estimate flow velocity using a different relation given by Chow (1959) that is based on superelevation, the elevation difference of a channelized deposit between the inside and outside of a curve (e.g., Evans et al., 2001; Vallance and Scott, 1997; Voight and Sousa, 1994):

$$v = [d(r/w)g]^{0.5}, \tag{2}$$

where v is velocity in meters per second, d is superelevation in meters, r is curve radius in meters, w is channel width in meters, and g is gravitational accele-

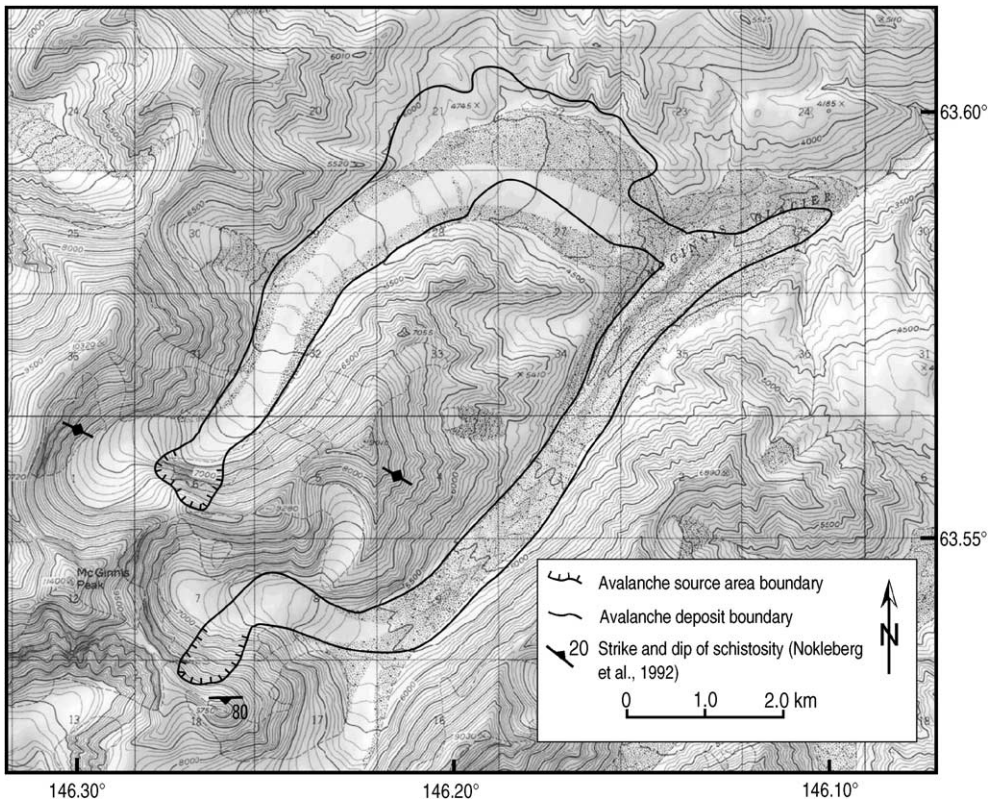

Fig. 4. Map showing McGinnis Peak rock avalanches. Topographic base from USGS Mt. Hayes (C-5) quadrangle, original scale 1 : 63,360, contour interval 100 ft (30 m), datum mean sea level. Strikes and dips of schistosity from Nokleberg et al. (1982).

ration. This equation was developed assuming that gravitational force balances the centrifugal force that causes a flow to climb the outside wall of a curved channel. Only gravitational force is considered to resist flow, as with Eq. (1); therefore, the minimum velocity is estimated. For a 60-m super-elevation, a curve radius

Fig. 5. McGinnis Peak rock avalanches (view toward southwest). Two rock avalanches were triggered from the north (N) and south (S) flanks of McGinnis Peak. The rock avalanches both traveled on glacial surfaces and merged in the left center of the photo. The Denali Fault lies 9 km to the south.

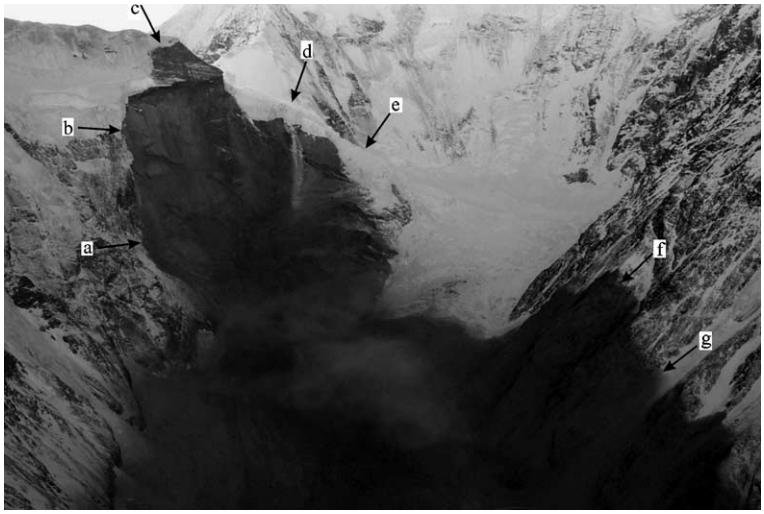

Fig. 6. Source area of McGinnis Peak rock avalanche (view toward southwest). The source is defined by pre-existing discontinuities in the rock mass. The main scarp is indicated by arrows a–e. Several meters of glacial ice also failed, as visible at arrows d and e; ice is avalanching down the scar below arrow d. The dark area indicated by arrows f and g marks a line of dust that was pushed in front of the rapidly moving slide mass.

of 3580 m, and a channel width of 1300 m, Eq. (2) yields a velocity of 40 m/s or about 150 km/h. These two velocity estimates are consistent with other reported velocity estimates of seismically induced rock avalanches that have moved at speeds as great as 250–300 km/h (Plafker et al., 1971).

Material exposed on the surface of the landslide deposit consists mainly of angular rock fragments having a fairly uniform distribution of grain sizes ranging from large boulders several meters on a side to fine-grained, soil-like material. The surface of the deposit also has ridges and depressions of several meters amplitude that reflect the flowage of the mass. Ridges in the interior part of the deposit tend to be perpendicular to the flow direction and to be convex downslope. Along the margins of the slide, ridges tend to parallel the margins and thus the direction of flow. These ridges and depressions make the surface of the deposit highly irregular and very difficult to traverse.

On the inside part of the turn where the rock avalanche followed the glacier and turned to the east, possible older landslide deposits are exposed on the glacier surface. The margin of the 2002 deposit is somewhat inboard (toward the inside part of the turn) of the midline of the glacier and is marked by a steep, well-defined margin 2–3 m high. This 2002 material was deposited on possible older landslide deposits that extend toward the inside of the turn (Fig. 8). Our brief field inspection indicated that two and possibly three successively older deposits are exposed moving inward

Fig. 7. McGinnis Peak rock-avalanche deposit (view toward north). Arrows mark edge of deposit. As the rock avalanche turned this corner, the outboard edge of the avalanche (upper center) flowed about 60 m up the outside valley wall. On the inboard edge of the corner, the deposit came to rest on older rock-avalanche deposits, visible in lower right corner of photo below the arrows.

Fig. 8. The 2002 rock-avalanche deposit has a steep, well-defined margin that extends left to right through the center of the photo (man inside circle shows scale, view toward northwest). The 2002 deposit (upper center of photo) came to rest on the material visible in the foreground, whose texture, lithology, and morphology are similar to those of the 2002 deposit, suggesting a similar origin. The material in the foreground, however, appears much older and suggests an older landslide event possibly triggered by a previous earthquake.

from the margin of the 2002 deposit. The morphology, texture, and lithology of the recent (2002) and older deposits are identical, suggesting similar origins. The multiple older deposits appear to differ in age from each other based on degree of revegetation on the surface of the deposits, degree of weathering, and geomorphic features such as stone lines suggesting old flow boundaries.

A second rock avalanche was triggered from a source area on a ridge extending southeast from McGinnis Peak (see Figs. 4 and 5). This failure involved more than 11×10^6 m^3 of material similar to that described above (Table 1). The landslide material covered virtually the entire surface of the southeastern lobe of the McGinnis Glacier, on which it traveled. The glacial surface was previously covered with rock debris, presumably from previous rock avalanches or smaller landslides from the valley margins, and the November 2002 landslide covered the surface with an average depth of 2 m of new rock debris.

The two rock avalanches converged where the two lobes of the glacier converge, and both then continued to travel to the snout of the glacier. Thus, the two rock avalanches each had travel distances of 11–12 km.

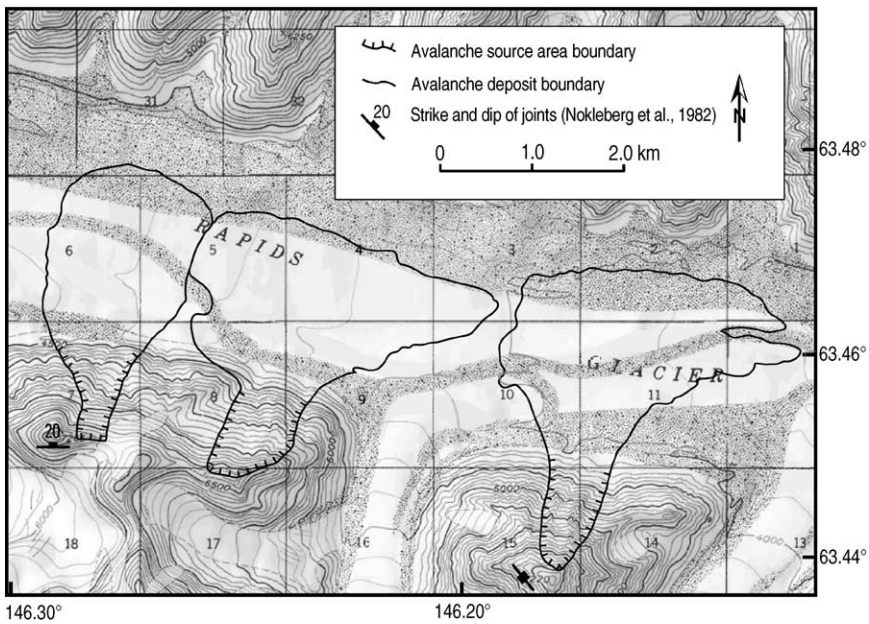

Fig. 9. Map showing Black Rapids rock avalanches. Topographic base from USGS Mt. Hayes (B-5) quadrangle, original scale 1:63,360, contour interval 100 ft (30 m), datum mean sea level. Strikes and dips of joints from Nokleberg et al. (1982).

4.2. Black Rapids rock avalanches

The 2002 earthquake triggered three large and several smaller rock avalanches from steep granitic slopes that form the southern edge of the valley occupied by the Black Rapids Glacier (Figs. 1 and 9). The Denali Fault extends through this valley, and so the landslides occurred within a few hundred meters of the fault trace and buried the fault rupture in places. The three largest landslides had a combined volume of about 37×10^6 m^3 (Table 1). They cascaded down steep rock slopes, crossed a lateral moraine and a medial moraine, and then spread out about 2.5 km across the glacier-filled valley, coming to rest near the opposite valley wall (Fig. 10).

Multiple joint surfaces both subparallel and orthogonal to the slope face were exposed at the landslide sources. These joint surfaces defined slabs 30–50 m thick that failed and cascaded down the 35–38° slopes. The fractures that defined the basal failure surfaces of the two western landslides extended beneath the ridge top and daylighted on the back side of the slope; thus, the entire ridge top failed, and the main scarps define scallops in the ridge line where the previous ridge top is now missing. On the back side of the ridge, an uphill-facing scarp having about 2 m

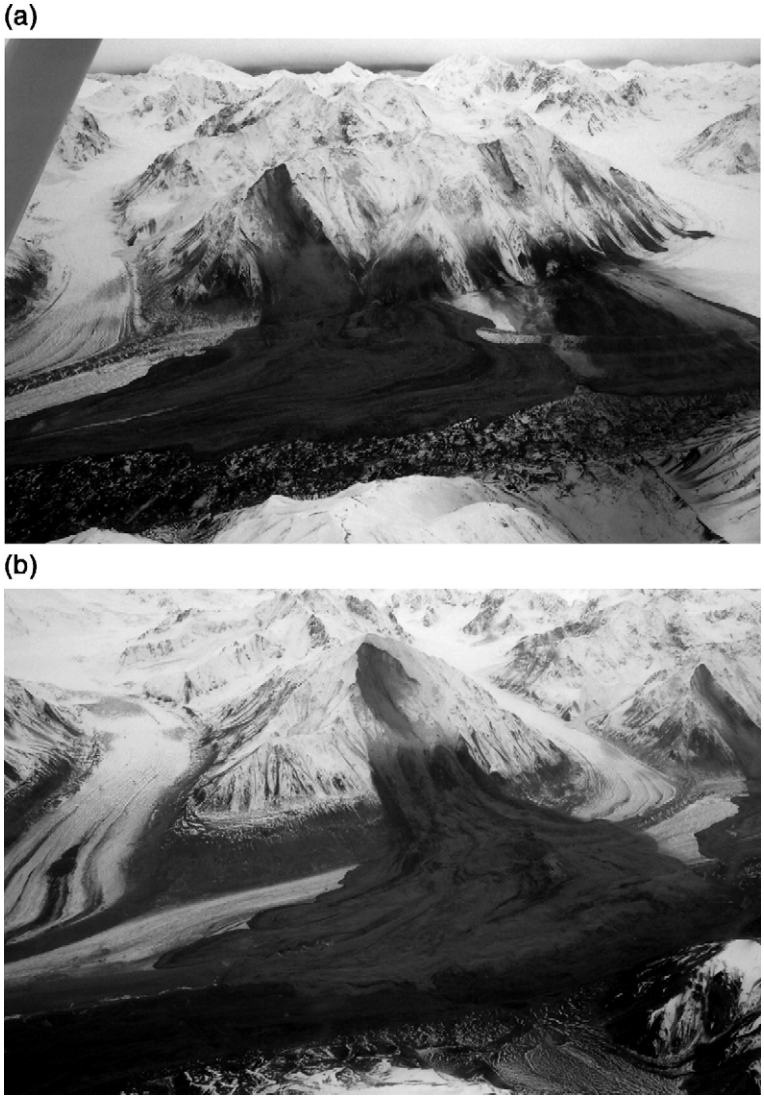

Fig. 10. Black Rapids rock avalanches (views toward south). The valley glacier is about 2-km wide here. The Denali Fault extends beneath the glacier near the mountain front. (a) Westernmost rock avalanches; note several smaller landslides extending along the ridge to the right. (b) Eastern rock avalanche; note multiple lobes of material that moved semi-independently of each other.

of northward displacement extends for tens of meters westward from the intersection of one of the main scarps and the new ridgeline. This fracture defines a much larger incipient failure mass that moved during the earthquake but did not fail catastrophically. This incipient failure mass of perhaps 100×10^6 m^3 could be reactivated in future earthquakes, heavy rainfall, or snowmelt episodes. The easternmost of the three landslides occurred on a ridge separated by a valley glacier from the ridge on which the other two occurred. The landslide scar is very similar to the other two; however, it extends to just below the mountain peak. Fractures visible in the source area indicate that the entire peak forms an incipient failure that could be similarly reactivated.

The deposits were uniformly thin, about 3 m in most areas, including where the avalanche debris spread up and over a 50 m high medial moraine. Eq. (1) indicates that the avalanches were moving at least 130 km/h to cross the moraine, but they were certainly moving faster as they then traveled more than 2 km down the 1–2° sloped glacial surface.

Two of the rock avalanches crossed the glacier and then turned and flowed some hundreds of meters down the valley on the glacier surface. From a distance, the surface of the deposits appears to have a homogeneous texture, but the surface is banded where flow features formed in the blocky debris (Fig. 11). Walking on the deposits, however, was very difficult owing to the blocky surface. The grain-size distribution of the deposits is continuous across a broad range, from clayey and silty soil to granitic blocks several meters on a side. The margins of the deposits are sharply defined, have nearly uniform inclination of 38°, and average 2–3 m in height.

4.3. West Fork rock avalanches

Two large rock avalanches were triggered above the West Fork Glacier (see Fig. 1) from steep slopes in two adjacent glacial cirques (Fig. 12, Table 1). The dislodged rock moved rapidly down the cirques, crossed the lateral moraine at the edge of the valley, and spread out as it flowed onto the glacial surface (Fig. 13). The north slide is 3.3-km long and averages 700-m wide; the south slide is 4.1-km long and about 800-m wide.

Landslide material failed from multiple sources on the steep slopes of the cirques. Slopes adjacent to the source areas were deeply fissured, and large parts of these slopes partially mobilized, leaving incipient landslide masses perched on the slopes. Large amounts of the rock-avalanche debris came to rest in the bottoms of the cirques and created convex-upward deposits that covered whatever glacial ice was still in the cirques.

The lower parts of the deposits on the glacier surface consisted mainly of blocks of fine-grained metamorphic rock spanning a wide range of sizes; some individual blocks measured more than 20 m on a side (Fig. 14). The thickness of the deposits generally ranged between 3 and 15 m, thinner where smaller blocks accumulated and thicker where large blocks came to rest. The deposits had sharp, steep margins. In most places, even large blocks on the leading edge of the toe appeared to have

Fig. 11. Deposit of middle Black Rapids rock avalanche (view toward northwest). Note the uniform thickness and sharp edge of the deposit. Bands on surface of deposits indicate flow of different lobes of material. The glacier is about 2-km wide here. The moraine extending horizontally through the lower part of the photo is about 15 m high.

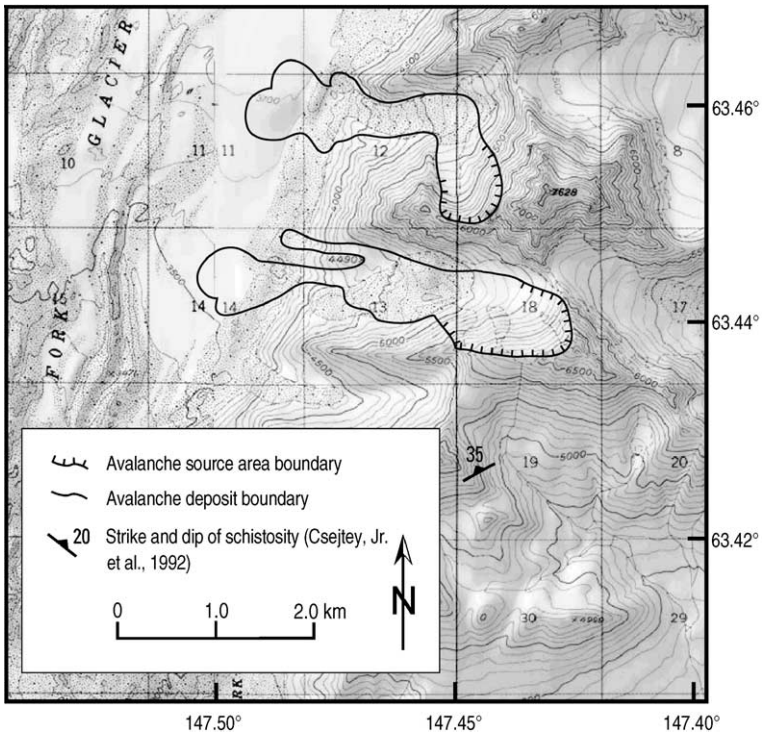

Fig. 12. Map showing West Fork Glacier rock avalanches. Topographic base from USGS Healy (B-1) quadrangle, original scale 1:63,360, contour interval 100 ft (30 m), datum mean sea level. Strike and dip of schistosity from Csejtey et al. (1992).

slid across the glacial ice with little gouging of the surface.

Each of the two rock avalanches had a volume of about $2–3 \times 10^6$ m^3 on the glacier surface, and we estimate that a substantial amount of landslide debris remains upslope in the cirques. The south rock avalanche had a significantly longer path covered with debris, thus we estimate that the total volumes of the north and south landslides were 4.1×10^6 and 4.4×10^6 m^3, respectively.

These rock avalanches showed evidence of high-speed travel. For example, one of them deposited land-

Fig. 13. West Fork Glacier rock avalanches (view toward east). The surface trace of the Susitna Glacier Fault lies on the far side of the mountains in the foreground. Glacier is 3–4-km wide here.

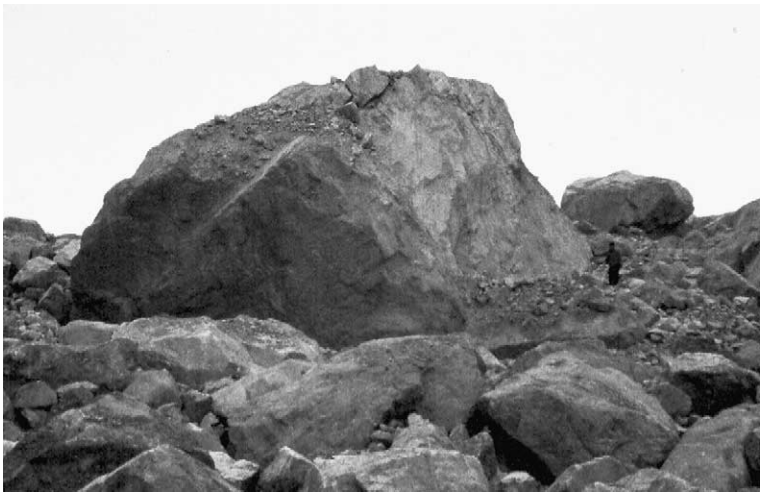

Fig. 14. Large block in deposit of West Fork Glacier rock avalanche. Blocks of this size were numerous and indicated the presence of fairly massive rock in the source area.

slide debris on a surface about 50 m above the bottom of the cirque on the wall opposite the source area. From Eq. (1), the velocity here was at least 113 km/h. Also, parts of the lee side of the lateral moraine crossed by the rock avalanche were undisturbed, indicating that at least some of the avalanche debris may have been airborne to avoid disturbing this part of the moraine.

5. Discussion

With few seismic instruments in this region, the pattern of landsliding may be one of the best indicators of the pattern of ground shaking. Keefer's (2002) relationship between area affected by landslides and earthquake magnitude shows that the mean area affected by a **M** 7.9 earthquake is approximately 28,000 km^2, and the maximum area is about 90,000 km^2. Based on the landslide distribution shown in Fig. 1, the area within which nearly all the landslides occurred in the 3 November earthquake measures only 10,000 km^2, which is roughly on the lower boundary of Keefer's (2002) data. This relatively small area affected by landslides suggests lower than average ground shaking in this earthquake. In contrast, the area affected by landslides triggered by the 1964 Alaska earthquake of **M** 9.2 was 269,000 km^2, and the farthest landslides were triggered 700 km from the epicenter (Plafker et al., 1969; Keefer, 1984, 2002).

Abnormally dry conditions can also inhibit landsliding during earthquakes (Keefer and Manson, 1998), but this appears not to have been a factor in the Denali Fault earthquake. Regional climatological records for the areas around the fault-rupture zone indicate that annual precipitation for 2002 was 40–50 mm above normal (National Oceanic and Atmospheric Administration, 2002).

The pattern of landsliding suggests that shaking levels necessary to trigger rock falls and rock slides generally were focused in a narrow band centered along the fault zone rather than extending radially outward for great distances. And even within this zone, the number and concentration of these slides appeared less than would be expected for an earthquake of this magnitude. Keefer (2002) indicated that earthquakes in this magnitude range might be expected to trigger an average of 80,000 landslides in the epicentral area, but in the 2002 earthquake the concentration appeared to be at least an order of magnitude less than this.

Few landslides were triggered west of the epicenter; most of the landslides, including the large rock avalanches, occurred east of the epicenter. This pattern is clearly consistent with the eastward propagation of the second and third subevents of the earthquake (Eberhart-Phillips et al., 2003). West of the epicenter, areas of concentrated rock falls and rock slides disappear within 30 km of the epicenter, whereas to the southeast, the zone of concentrated rock falls and rock slides extends more than 300 km along the fault-rupture zone.

Failures in brittle rock are most sensitive to high accelerations commonly within the higher frequencies (1–10 Hz) of ground motion. Relative to other earthquakes of comparable or lower magnitudes (1987 Ecuador M 6.9; 1970 New Guinea M 7.1; 1976 Darien, Panama M 7.0; 1977 San Juan, Argentina M 7.4; 1970 Peru M 7.9) for which landslide concentrations have been measured or estimated (Keefer, 1993), the

Denali earthquake had significantly lower concentrations of rock falls and rock slides. The epicentral area along the Denali and Totschunda Faults contains abundant steep slopes in highly fractured and sheared materials that should be highly susceptible to failure during seismic shaking. Thus, the relatively low concentrations of rock falls and rock slides suggest that the earthquake shaking was deficient in high-frequency energy and high peak accelerations. Although the paucity of near-field instrumental data make such conclusions tentative, the one near-field strong-motion instrument (Pump Station 10, about 3 km north of the fault rupture along the Richardson Highway, see Fig. 1) recorded a maximum horizontal acceleration of only 0.36 *g*, a rather modest peak acceleration for an earthquake of this magnitude (Ellsworth et al., 2004). Frankel (2004) notes that this recording may not be representative of near-field ground motions because of its location midway between subevent 1, which likely produced the highest near-field accelerations, and subevent 3, which had the greatest moment release. Ellsworth et al. (2004) note, however, that analysis of the Pump Station 10 record suggests reduced high-frequency motion possibly due to super-shear rupture velocity.

For comparison, the 1994 Northridge, California, earthquake (**M** 6.7) produced accelerations exceeding 1 *g* and triggered more than 11,000 landslides with concentrations of hundreds of slides per square kilometer (Harp and Jibson, 1995, 1996). Because the first subevent of the Denali Fault earthquake was a **M** 7.2 thrust, we would have expected to see similar landslide concentrations there as we saw from the Northridge earthquake. Although a few large rock avalanches were triggered in this area, we were surprised that the overall concentrations of landslides were significantly lower than those triggered by the Northridge earthquake, despite the fact that the Northridge earthquake was much deeper on a blind fault (Wald et al., 1996). In fact, the 2002 rock avalanches were separated by large areas of only sparse landslide activity despite the presence of abundant steep slopes in what appeared to be similarly susceptible rock.

Inversion studies by Frankel (2004) indicate that subevent 1 (the thrust event) produced by far the largest high-frequency (1–10 Hz) energy release per unit fault length. High-frequency energy moderated along the subevent 2 segment, which may in part explain the moderate ground acceleration recorded at Pump Station 10. Subevent 3, despite having the highest moment release and greatest surface slip, was relatively deficient in high-frequency energy, and the rupture of the Totschunda Fault generated negligible high-frequency energy. Frankel et al. (2002) also showed that subevents 1 and 2 contained the highest accelerations within the earthquake records. These conclusions are strikingly consistent with the observed landslide distribution: all of the largest landslides clustered between the first two subevents, where accelerations and high-frequency energy were highest, and landslide concentration decreased gradually eastward along the fault-rupture zone.

The **M** 7.2 thrust that formed the first subevent probably played a major role in the triggering of the large rock avalanches, particularly those on the West Fork Glacier. The West Fork Glacier rock avalanches were on the hanging wall directly above the thrust fault, a location that has been correlated with abnormally high ground motions in past earthquakes (Abrahamson and Somerville, 1996; Dalguer et al., 2001). Also, thrust earthquakes generally have higher frequency ground motion and higher accelerations than strike-slip events of similar magnitudes (Abrahamson and Silva, 1997; Boore et al., 1997; Somerville et al., 1996).

Farther to the east, the absence of large landslides near subevent 3 and along the Totschunda Fault (Fig. 1) suggests that shaking levels were lower there. Along this eastern part of the fault zone the topography has a somewhat softer texture—owing to the presence of more erodible sedimentary rock—than in the areas near subevents 1 and 2, but very steep slopes in weak material susceptible to slope failure are still abundant in this eastern zone. For example, about 15 km west of Gillett Pass, a series of very large, ancient rock-avalanche deposits extends for several kilometers along the valley floor along the Denali fault trace. Thus, these slopes have produced rock avalanches even larger than those triggered to the west in 2002, but shaking conditions in 2002 along this part of the fault were not severe enough to trigger large landslides.

The area around the rock avalanches at Black Rapids Glacier and McGinnis Peak has high relief and many steep slopes of all orientations. All five of the large rock avalanches, however, occurred on nearly identically oriented north–northeast-facing slopes. This suggests that there may have been a large north–northeastward (fault-normal) component of ground motion associated with subevent 1 and (or) 2.

Comparison of landslides and liquefaction effects casts further light on the strong-motion distribution produced by the earthquake. Whereas both liquefaction and landslides occurred within the 30-km-wide zone that parallels the fault rupture, the liquefaction effects also extended significantly beyond this zone, which is unusual when compared with other earthquakes. Keefer's (1984) data from 40 worldwide earthquakes show

that epicentral and fault-rupture distance limits for liquefaction-induced landslides are below those of other types of landslides across all earthquake magnitudes. Further, the concentration of the large rock avalanches near the first two subevents is also in contrast with the broad eastward concentration of liquefaction effects in the area of the third subevent of the earthquake. In the eastern part of the area, liquefaction effects were much more extensive and deformation more severe than in areas to the west near the first and second subevents (Fig. 1; Kayen et al., 2004), despite the presence of abundant areas highly susceptible to liquefaction throughout the entire epicentral region.

We attribute the contrast in the landslide and liquefaction occurrences to the fact that landslides and liquefaction effects are sensitive to different ground-shaking parameters. Failures in brittle rock are sensitive to high accelerations commonly within the higher frequencies of ground motion. Rock failures can be triggered by very short durations of high accelerations. Liquefaction-induced failure of saturated sediment, on the other hand, is most responsive to longer period ground shaking and depends more on shaking duration than on short pulses of high acceleration; repetitive cycles of shear strain are required to trigger liquefaction (Seed and Lee, 1966). Thus, the concentration of severe liquefaction occurrences in the eastern part of the area suggests longer durations and periods of shaking there. The third subevent, which occurred nearest to most of the severe liquefaction locations, produced the longest fault rupture and the greatest fault offsets, which could relate to longer shaking durations. The third subevent also produced lower frequency ground motions than the first two subevents (Choy and Boatwright, 2004; Frankel, 2004). Indeed, although the high-frequency response at Pump Station 10 was modest, the long-period response was substantial (Ellsworth et al., 2004).

The long-runout distances of some of the rock avalanches merit examination. We compared the runout distances of the McGinnis Peak, Black Rapids, and West Fork rock avalanches with those of other rock avalanches worldwide (Evans and Clague, 1988; Shaller, 1991). Fig. 15 plots the log of landslide volume versus the length (runout) to height (total vertical drop) ratio of 145 landslides that traveled on the ground and 38 that traveled on ice (glacial surfaces). Interestingly, most of the data cluster together regardless of substrate. The Denali Fault earthquake rock avalanches plot within, but on the long-runout side of, the overall data cluster and on the long-runout edge of the data for

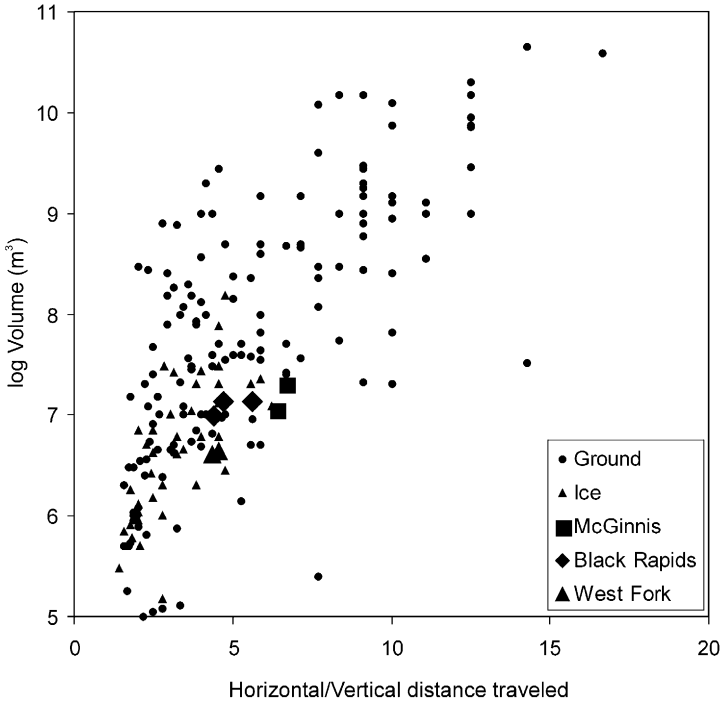

Fig. 15. Plot comparing volumes of rock avalanches with the ratio of their horizontal to vertical travel distance. Rock avalanches traveling on ice (glacial surfaces) and ground generally cluster together. Rock avalanches triggered by the 2002 earthquake plot within, but on the long-runout side of, the worldwide data. Data from Evans and Clague (1988) and Shaller (1991).

landslides on ice. This comparison indicates that these landslides had relatively long—but not exceptional—runout distances.

The older landslide deposits exposed on the McGinnis Glacier are of particular interest because they indicate that what occurred during the 2002 earthquake could be a repeat of similar events in the past. The similarity in morphology, lithology, and texture of these older deposits with the 2002 deposit certainly suggests a similar mechanism of deposition. If these previous landslides were also triggered by earthquake shaking, dating the older deposits could indicate the timing of earlier earthquakes. Although proving a seismic origin for these older deposits might be difficult, such an origin might reasonably be assumed because of the similarities in size, texture and morphology of the older and recent deposits (Jibson, 1996a,b).

The well-preserved flow features, long runout, and relatively uniform thickness of the rock-avalanche deposits, particularly those on Black Rapids Glacier, provide interesting insights into the physics of these flows. The material, despite being composed of coarse, blocky rock fragments, behaved as a viscous fluid as it flowed. A detailed analysis of this phenomenon is beyond the scope of this paper and will be the subject of a subsequent article.

6. Summary and conclusions

The Denali Fault earthquake of 3 November 2002 triggered thousands of landslides, primarily rock falls and rock slides, that formed an unusual pattern. Unlike landslide distributions in most previous earthquakes, the triggered slides clustered in a narrow band about 30-km wide along the more than 300-km fault-rupture zone. Several large rock avalanches 4–20 $\times 10^6$ m^3 in volume also were triggered, and some of these traveled more than 11 km on the surfaces of valley glaciers. Several inferences about the strong shaking can be drawn from analysis of the distribution of triggered landslides, and these inferences have since been confirmed independently by various seismological studies:

1. The low concentration of landslides in the near field suggests that the earthquake was deficient in high-frequency energy and attendant high accelerations. The single near-field acceleration recording, which admittedly may not be representative, was only 0.36 *g*.
2. Accelerations high enough to trigger landslides extended relatively short distances, only about 15 km, from the zone of fault rupture.
3. The clustering of large rock avalanches within the areas of the first two subevents of the earthquake is consistent with these subevents containing the highest accelerations and greatest amount of high-frequency energy of the earthquake record. No large rock avalanches were present in the area of the third subevent, which generated large fault displacements but relatively lower accelerations and less high-frequency energy.
4. Landslides extended only short distances to the west of the epicentral area of the earthquake whereas to the east they extended for more than 300 km along the zone of fault rupture, presumably because of eastward directivity of shaking that attended the eastward propagation of fault rupture.
5. Liquefaction features were primarily concentrated in the eastern part of the epicentral area well beyond the zone of concentrated landslides. This could have been an effect of a longer duration and period of shaking in the third subevent.
6. The presence of older rock-avalanche deposits that are similar to the 2002 deposits indicates that what happened in 2002 was a repeat of earlier, similar events. Dating these deposits could provide insight into the timing of earlier earthquakes.

Soon after the earthquake, we suggested that the distribution of triggered ground failures (landslides and liquefaction) could tell us something about the characteristics of the near-field ground motions (Eberhart-Phillips et al., 2003; Harp et al., 2003). The consistency of these early hypotheses with the results of later seismological (Choy and Boatwright, 2004; Ellsworth et al., 2004; Frankel, 2004) and geotechnical (Kayen et al., 2004) studies, as discussed in detail in this paper, demonstrates the usefulness of detailed characterization and analysis of post-earthquake ground-failure distributions. Certainly in areas where near-field strong-motion instruments are absent or sparse, analysis of the distribution of shaking-induced ground failures can play a key role in interpreting—even if only with a broad brush—near-field ground motions.

References

Abrahamson, N.A., Silva, W.J., 1997. Empirical response spectral attenuation relations for shallow crustal earthquakes. Seismol. Res. Lett. 68, 94–127.

Abrahamson, N.A., Somerville, P., 1996. Effects of the hanging wall and footwall on ground motions recorded during the Northridge earthquake. Seismol. Soc. Am. Bull. 86 (1B), S93–S99.

Boore, D.M., Joyner, W.B., Fumal, T.E., 1997. Equations for estimating horizontal response spectra and peak acceleration from

western North American earthquakes: a summary of recent work. Seismol. Res. Lett. 68, 128–153.

Chow, V.T., 1959. Open-Channel Hydraulics. McGraw-Hill, New York. 680 pp.

Choy, G.L., Boatwright, J., 2004. Radiated energy and the rupture process of the Denali Fault earthquake of 2002 from broadband teleseismic body waves. Seismol. Soc. Am. Bull. 94 (6B), S269–S277.

Csejtey Jr., B., Mullen, M.W., Cox, D.P., Stricker, G.D., 1992. Geology and geochronology of the Healy quadrangle, south-central Alaska. U.S. Geol. Surv. Misc. Investigations Map I-1961, scale 1:250,000.

Dalguer, L.A., Irikura, K., Riera, J.D., Chiu, H.C., 2001. The importance of the dynamic source effects on strong ground motion during the Chi-Chi, Taiwan, earthquake: brief interpretation of the damage distribution on buildings. Seismol. Soc. Am. Bull. 91, 1112–1127.

Eberhart-Phillips, D., Haeussler, P.J., Freymueller, J.T., Frankel, A.D., Rubin, C.M., Craw, P., Ratchkovski, N.A., Anderson, G., Carver, G.A., Crone, A.J., Dawson, T.E., Fletcher, H., Hansen, R., Harp, E.L., Harris, R.A., Hill, D.P., Hreinsdóttir, S., Jibson, R.W., Jones, L.M., Kayen, R., Keefer, D.K., Larsen, C.F., Moran, S.C., Personius, S.F., Plafker, G., Sherrod, B., Sieh, K., Sitar, N., Wallace, W.K., 2003. The 2002 Denali Fault earthquake, Alaska: a large magnitude, slip-partitioned event. Science 300, 1113–1118.

Ellsworth, W.L., Celebi, M., Evans, J.R., Jensen, E.G., Kayen, R., Metz, M.C., Nyman, D.J., Roddick, J.W., Spudich, P., Stephens, C.D., 2004. Near-field ground motion of the 2002 Denali fault, Alaska, earthquake recorded at pump station 10. Earthq. Spectra 20, 597–615.

Evans, S.G., Clague, J.J., 1988. Catastrophic rock avalanches in glacial environments. In: Bonnard, C. (Ed.), Proceedings, 5th International Symposium of Landslides, Lausanne, Switzerland, vol. 2, pp. 1153–1159.

Evans, S.G., Hungr, O., Clague, J.J., 2001. Dynamics of the 1984 rock avalanche and associated distal debris flow on Mount Cayley, British Columbia, Canada; implications for landslide hazard assessment on dissected volcanoes. Eng. Geol. 61, 29–51.

Frankel, A.D., 2004. Rupture process of the M 7.9 Denali fault, Alaska, earthquake: subevents, directivity, and scaling of high-frequency ground motions. Seismol. Soc. Am. Bull. 94 (6B), S234–S255.

Frankel, A.D., Biswas, N.N., Martirosyan, A.H., Dutt, U., McNamara, D.E., 2002. Rupture process of the M 7.9 Denali Fault, Alaska, earthquake determined from strong-motion recordings. EOS, Trans. Am. Geophys. Union 47, 1340.

Haeussler, P.J., Schwartz, D.P., Dawson, T.E., Stenner, H.D., Lienkaemper, J.J., Cinti, F., Montone, P., Sherrod, B., Craw, P., 2004. Surface rupture of the 2002 Denali fault, Alaska, earthquake and comparison with other strike-slip ruptures. Earthq. Spectra 20, 565–578.

Hansen, R.A., Ratchkovski, N.A., 2004. Seismological aspects of the 2002 Denali Fault, Alaska, earthquake. Earthq. Spectra 20, 555–563.

Harp, E.L., Jibson, R.W., 1995. Inventory of Landslides Triggered by the 1994 Northridge, California Earthquake. U. S. Geol. Surv. Open-File Report 95-213. 17 pp.

Harp, E.L., Jibson, R.W., 1996. Landslides triggered by the 1994 Northridge, California earthquake. Seismol. Soc. Am. Bull. 86 (1B), S319–S332.

Harp, E.L., Jibson, R.W., Kayen, R.E., Keefer, D.K., Sherrod, B.L., Carver, G.A., Collins, B.D., Moss, R.E.S., Sitar, N., 2003. Landslides and liquefaction triggered by the M 7.9 Denali Fault earthquake of 3 November 2002. GSA Today 13 (8), 4–10.

Jibson, R.W., 1996a. Use of landslides for paleoseismic analysis. Eng. Geol. 43, 291–323.

Jibson, R.W., 1996b. Using landslides for paleoseismic analysis. In: McCalpin, J.P. (Ed.), Paleoseismology. Academic Press, Inc., San Diego, pp. 397–438.

Jibson, R.W., Harp, E.L., Schulz, W., Keefer, D.K., 2004. Landslides triggered by the 2002 M-7.9 Denali Fault, Alaska, earthquake and the inferred nature of the strong shaking. Earthq. Spectra 20, 669–691.

Kayen, R.E., Thompson, E., Minasian, D., Moss, R.E.S., Collins, B.D., Sitar, N., Dreger, D., Carver, G.A., 2004. Geotechnical reconnaissance of the November 3, 2002 M 7.9 Denali Fault Earthquake. Earthq. Spectra 20, 639–667.

Keefer, D.K., 1984. Landslides caused by earthquakes. Geol. Soc. Amer. Bull. 95, 406–421.

Keefer, D.K., 1993. The susceptibility of rock slopes to earthquake-induced failure. Assoc. Eng. Geol. Bull. 30, 353–361.

Keefer, D.K., 2002. Investigating landslides caused by earthquakes—a historical review. Surv. Geophys. 23, 473–510.

Keefer, D.K., Manson, M.W., 1998. Regional distribution and characteristics of landslides generated by the earthquake. In: Keefer, D.K. (Ed.), The Loma Prieta, California, earthquake of October 17, 1989—Landslides, U.S. Geol. Surv. Prof. Pap., vol. 1551-C, pp. 7–32.

Kikuchi, M., Yamanaka, Y., 2002. Source Rupture Processes of the Central Alaska Earthquake of Nov. 3, 2002, Inferred from Teleseismic Body Waves (the 10/23 M6.7 event). EIC Seismological Note No. 129.

Martirosyan, A., Hansen, R.A., Ratchkovsky, N.A., 2004. Strong-motion records of the 2002 Denali fault, Alaska, earthquake. Earthq. Spectra 20, 579–596.

Miller, M.L., Bradley, D.C., Bundtzen, T.K., McClelland, W., 2002. Late Cretaceous through Cenozoic strike-slip tectonics of southwestern Alaska. J. Geol. 110, 247–270.

National Oceanic and Atmospheric Administration, 2002. Climatological Data—Annual Summary, Alaska 2002, vol. 88(13), pp. 4–9.

Nokleberg, W.J., Albert, N.R.D., Bond, G.C., Herzon, P.L., Miyaoka, R.T., Nelson, W.H., Richter, D.H., Smith, T.E., Stout, J.H., Yeend, W., Zehner, R.E., 1982. Geologic map of the southern part of the Mount Hayes quadrangle, Alaska. U.S. Geol. Surv. Open-File Report 82-52, scale 1:250,000.

Plafker, G., Kachadoorian, R., Eckel, E.B., Mayo, L.R., 1969. Effects of the earthquake of March 27, 1964 on various communities. U. S. Geol. Surv. Prof. Pap. 542-G (50 pp).

Plafker, G., Ericksen, G.E., Fernández, C.J., 1971. Geological aspects of the May 31, 1970, Peru earthquake. Seismol. Soc. Am. Bull. 61, 543–578.

Plafker, G., Hudson, T., Richter, D.H., 1977. Preliminary observations on late Cenozoic displacements along the Totschunda and Denali Fault systems. U.S. Geol. Surv. Circ. 751-B, B67–B69.

Plafker, G., Gilpin, L.M., Lahr, J.C., 1994. Neotectonic map of Alaska. In: Plafker, G., Berg, H.C. (Eds.), The Geology of Alaska. Geol. Soc. Am., Boulder, CO. plate 12.

Post, A., 1967. Effects of the March 1964 Alaska earthquake on glaciers. U. S. Geol. Surv. Prof. Pap. 554-D (42 pp.).

Seed, H.B., Lee, K.L., 1966. Liquefaction of saturated sands during cyclic loading. Am. Soc. Civil Engr. Jour. Soil Mech. Foundations Div., vol. 92, SM6, pp. 105–134.

Shaller, P.J., 1991. Analysis and implications of large Martian and terrestrial landslides. Ph.D. Dissertation, Calif. Inst. Tech., p. 586.

Somerville, P., Saikia, C., Wald, D., Graves, R., 1996. Implications of the Northridge earthquake for strong ground motions from thrust faults. Seismol. Soc. Am. Bull. 86 (1B), S115–S125.

Tuthill, S.J., Laird, W.M., 1966. Geomorphic effects of the earthquake of March 27, 1964, in the Martin–Bering Rivers area, Alaska. U. S. Geol. Surv. Prof. Pap. 543-B, 1–29.

Vallance, J.W., Scott, K.M., 1997. The Osceola mudflow from Mount Rainier: sedimentology and hazard implications of a huge clay-rich debris flow. Geol. Soc. Amer. Bull. 109, 143–163.

Varnes, D.J., 1978. Slope movement types and processes. In: Schuster, R.L., Krizek, R.J. (Eds.), Landslides—Analysis and Control, Trans. Res. Board, Nat. Acad. Sci., Spec. Rep., vol. 176, pp. 11–33.

Voight, B., Sousa, J., 1994. Lessons from Ontake-san: a comparative analysis of debris avalanche dynamics. Eng. Geol. 38, 261–297.

Wald, D.J., Heaton, T.H., Hudnut, K.W., 1996. The slip history of the 1994 Northridge, California, earthquake determined from strong-motion, teleseismic, GPS, and leveling data. Seismol. Soc. Am. Bull. 86 (1B), S49–S70.